Quantum ratchet effects induced by terahertz radiation in GaN-based two-dimensional structures

W. Weber,[1] L. E. Golub,[2] S. N. Danilov,[1] J. Karch,[1] C. Reitmaier,[1] B. Wittmann,[1] V. V. Bel'kov,[2]
E. L. Ivchenko,[2] Z. D. Kvon,[3] N. Q. Vinh,[4] A. F. G. van der Meer,[4] B. Murdin,[5] and S. D. Ganichev[1*]

[1] *Terahertz Center, University of Regensburg, 93040 Regensburg, Germany*
[2] *A.F. Ioffe Physico-Technical Institute, Russian Academy of Sciences, 194021 St. Petersburg, Russia*
[3] *Institute of Semiconductor Physics, Russian Academy of Sciences, 630090 Novosibirsk, Russia*
[4] *FOM Institute for Plasma Physics "Rijnhuizen",*
P.O. Box 1207, NL-3430 BE Nieuwegein, The Netherlands and
[5] *University of Surrey, Guildford, GU2 7XH, UK*

Photogalvanic effects are observed and investigated in wurtzite (0001)-oriented GaN/AlGaN low-dimensional structures excited by terahertz radiation. The structures are shown to represent linear quantum ratchets. Experimental and theoretical analysis exhibits that the observed photocurrents are related to the lack of an inversion center in the GaN-based heterojunctions.

PACS numbers: 73.21.Fg, 78.67.De, 73.63.Hs

I. INTRODUCTION

In recent years, physics of quantum ratchets draw a growing attention. In mechanics, a ratchet is a device that is used to restrict motion in one direction while permitting it in another. In general, one means by a ratchet any sort of asymmetric potential, or a potential lacking a center of the spatial inversion. At the turn of 1980/90's it was understood that unbiased nonequilibrium noncentrosymmetric systems can generate transport of particles, and this conception has roots in different fields of physics, chemistry and biology. In mechanical, electronic, optical and biological systems, a particle, classical or quantum, charged or neutral, propagating in a periodic potential with broken centrosymmetry and subjected to an *ac* force exhibits a net *dc* macroscopic flow. Examples are electrons in solids, Abrikosov vortices in superconductors and biological motor proteins.[1] One of implementations of the ratchet phenomenon is a Linear Photo-Galvanic Effect (LPGE). It represents a generation of a *dc* electric current under absorption of linearly polarized light in unbiased crystals of piezoelectric classes. Glass et al.[2] were the first to attribute a photoinduced current observed in ferroelectric $LiNbO_3$ to a novel photogalvanic effect and propose the first correct model for its microscopic qualitative interpretation. A consistent quantitative theory of LPGE was developed by Belinicher and Sturman followed by other theorists, see Refs. 3,4.

Noncentrosymmetric bulk semiconductors and heterostructures are natural quantum ratchets and the further studies of LPGE in these systems allow one to elucidate the whole problem of the ratchet effect. In particular, a current of the LPGE consists of two contributions, ballistic and shift, which as a rule are comparable in the order of magnitude.[5] It is important to note that simi-lar two contributions to the electric current, called the skew-scattering and side-jump currents, do exist in the anomalous Hall effect, see the recent review by Sinitsyn.[6] Another important point is that one should include into the light absorption process contributing to the ballistic current an additional simultaneous scattering from a static defect or a phonon, as compared to the light-induced optical transition leading to the shift current. In GaN-based structures first observation of LPGE has been reported quite recently.[7,8,9,10,11,12] Here we present results of detailed experimental and theoretical investigation of LPGE in heterostructures based on GaN and its alloys with AlN. The commercial fabrication of blue and green LEDs have led to well established technological procedures of epitaxial preparation of these heterostructures and initiated a great activity on investigations of their properties.[13] The photogalvanics serves as a solid bridge between transport and optics and, therefore, reveals both transport and optical properties of the systems under study.

II. SAMPLES AND EXPERIMENTAL METHODS

The experiments are carried out on (0001)-oriented wurtzite n-GaN/$Al_{0.3}Ga_{0.7}N$ heterojunctions grown by MOCVD on C-plane sapphire substrates (for details of growth see Ref. 7). The thickness of the AlGaN layers was varied between 30 nm and 100 nm. An undoped 33 nm thick GaN buffer layer grown under a pressure of 40 Pa at temperature 550°C is followed by an undoped GaN layer ($\sim 2.5~\mu$m) grown under 40 Pa at 1025°C; the undoped $Al_{0.3}Ga_{0.7}N$ barrier was grown under 6.7 Pa at 1035°C. The mobility and density in the two-dimensional (2D) electron gas measured at room temperature are $\mu \approx 1200$ cm^2/Vs and $N_s \approx 10^{13}$ cm^{-2}, respectively. To measure the photocurrent two pairs of contacts are centered at opposite sample edges with the connecting
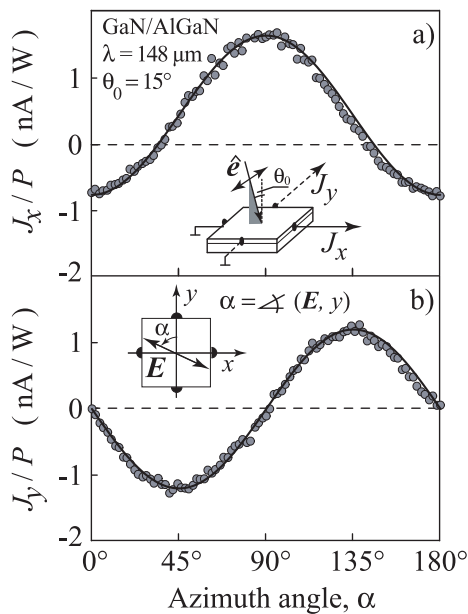
*e-mail: sergey.ganichev@physik.uni-regensburg.de

FIG. 1: Photocurrent as a function of angle α measured at room temperature at oblique incidence ($\theta_0 = 15°$) in the a) longitudinal (J_x) and b) transverse (J_y) geometries. Photocurrent is excited by linearly polarized radiation with wavelength $\lambda = 148$ μm and power $P \approx 5$ kW. Full lines are fits to Eqs. (6). To get agreement with experiments we used one fitting parameter $J_0 \propto \chi$ and introduced an offset J_{offset} for the current J_x detected in the direction of light propagation. The inset shows the experimental geometry. An additional inset in the lower panel displays the sample and the radiation electric field viewing from the source of radiation side.
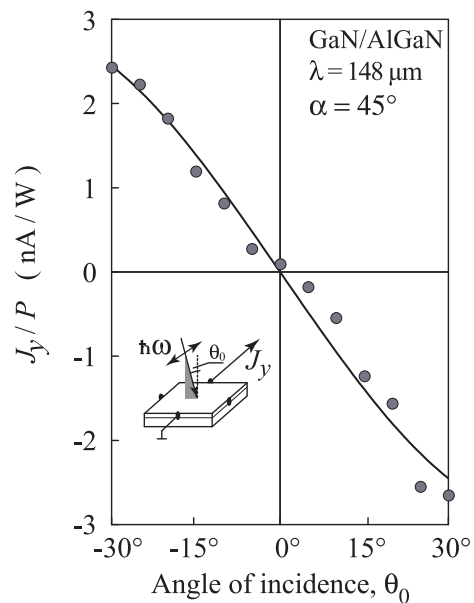

FIG. 2: Photocurrent as a function of angle of incidence θ_0 measured at room temperature in the transverse geometry and azimuth angle $\alpha = 45°$. Photocurrent is excited by radiation with wavelength $\lambda = 148$ μm and power $P \approx 5$ kW. Full line is the fit to Eqs. (6) with the same fitting parameter J_0 as used in Fig. 1. The inset shows the experimental geometry.

lines along the axes $x \parallel [1\bar{1}00]$ and $y \parallel [11\bar{2}0]$, see inset in Fig. 1. The current generated by the light in the unbiased samples is measured via the voltage drop across a 50 Ω load resistor in a closed-circuit configuration. The voltage is recorded with a storage oscilloscope.

The photocurrents were induced by indirect intrasubband (Drude-like) optical transitions in the lowest size-quantized subband. The emission from a terahertz (THz) molecular laser optically pumped by a TEA CO_2 laser[14] is used for the optical excitation. With NH_3, D_2O and CH_3F as an active media we could obtain radiation pulses of duration $\simeq$100 ns with wavelengths $\lambda = 77, 90.5, 148, 280, 385$ and 496 μm and a power $P \simeq 5$ kW. Radiation in both the normal- and oblique-incidence geometries were applied with the angle of incidence θ_0 varying from $-30°$ to $+30°$, $\theta_0 = 0$ corresponding to the normal incidence, and laser beam lying in the (xz) plane, see insets in Figs. 1, 2 and 4.

Optically pumped molecular lasers emit linearly polarized radiation with the polarization plane determined by that of the pump light: the electric field vector of the THz radiation E_l generated by the molecular laser can be either parallel (like for the lines $\lambda = 90.5, 148$ and 280 μm) or orthogonal (lines 77, 385 and 496 μm) to the polarization vector of the pump beam depending on the

angular momentum selection rules for the pump and the THz transitions in the active media.[14]

In the experiments the plane of polarization of the radiation incident on the sample was rotated applying $\lambda/2$ plates which enabled us to vary the azimuth angle α from $0°$ to $180°$ covering all possible orientations of the electric field component in the (xy) plane. Hereafter the angle $\alpha = 0$ is chosen in such a way that the incident light polarization is directed along the $y \parallel [11\bar{2}0]$ direction, see inset in Fig. 1(b).

To investigate the photogalvanic effects we also use elliptically polarized light. In this case the polarization of the laser beam is modified from linear to elliptical by means of crystal quartz $\lambda/4$ plates. The counterclockwise rotation (viewing from the laser side) of the optical axis of the quarter-wave plate by the angle φ_p results in the variation of the radiation helicity as $P_{\text{circ}} = -\sin 2\varphi_p$. Here the angle $\varphi_p = 0$ is chosen for the position of the quarter-wave plate optical axis coinciding with the incoming laser polarization, in which case the linear polarization degree is given by fourth harmonics of φ_p.

A series of measurements is carried out making use of the frequency tunability and short pulse duration of the free electron laser "FELIX" at FOM-Rijnhuizen in the Netherlands operated in the spectral range between 70 μm and 120 μm.[15] The output pulses of light from the FELIX were chosen to be ≈ 6 ps long, separated by 40 ns, in a train (or "macropulse") of 7 μs duration. The macropulses had a repetition rate of 5 Hz.

III. EXPERIMENTAL RESULTS

Irradiating the (0001)-grown GaN/AlGaN heterojunction by polarized light at oblique incidence, as sketched in the inset to Fig. 1(a), causes a photocurrent signal measured across a contact pair. The width of the photocurrent pulses is about 100 ns which corresponds to the THz laser pulse duration. The signal depends on the light polarization, and all characteristic polarization properties persist from 4.2 to 300 K. The experimental data presented below are obtained at room temperature. The effect is observed for all the wavelengths applied (between 77 μm and 496 μm). We use two geometries: the longitudinal geometry (J_x in the Fig. 1), in which the photocurrent is measured in the direction along in-plane component $\hat{e}_{\parallel}$ and the transverse geometry (J_y in the Fig. 1), where the signal is detected in the direction normal to the light propagation unit vector $\hat{e}$ [see the inset in Fig. 1(a)].

Figure 1 shows the dependence of the photocurrent on the azimuth angle α for both experimental geometries obtained at the positive incidence angle $\theta_0 = 15°$ and $\hat{e}_{\parallel} \parallel x$. The polarization dependence of the current in the longitudinal geometry is well fitted by $J_x = J_0(1 - \cos 2\alpha) + J_{\text{offset}}$ while for the transverse geometry we have $J_y = -J_0 \sin 2\alpha$. Note that the offset contribution J_{offset} is observed in the longitudinal geometry only. Below, in Sec. IV.B, we will demonstrate that exactly these dependences follow from the theory. As a function of the incidence angle the photocurrent changes sign at $\theta_0 \approx 0$. This is demonstrated in Fig. 2 which shows the dependence $J_y(\theta_0)$ for the fixed azimuth angle $\alpha = 45°$. A similar dependence is also detected for the longitudinal current J_x. We note that, like the polarization dependent contribution to the photocurrent, the detected offset current in the longitudinal geometry J_{offset} inverts its direction when the incidence angle changes its sign.

The wavelength dependence of the photocurrent obtained in transverse geometry at azimuth angle $\alpha = 135°$ and angle of incidence $\theta_0 = 15°$ is shown in Fig. 3. The data are measured both on FELIX (dots) and on molecular laser (triangles). Fitting the data to the well known spectral behavior of the Drude absorption[16,17]

$$J_y(\omega) \propto \eta(\omega) \propto \frac{1}{1 + (\omega\tau_p)^2} \qquad (1)$$

we obtain that the spectral behavior of the photocurrent can reasonably be described by this equation (see full line in Fig. 3). For the fit we used τ_p as an adjustable parameter and scaled the whole dependence by the ordinate. Analyzing this dependence we obtained that the momentum relaxation time controlling absorption is about 0.05 ps. This value is twice shorter than the transport time ($\simeq 0.1$ ps) extracted from the mobility measurements at room temperature. We attribute the shortening of the momentum relaxation time by electron gas heating due to absorption of the intense THz radiation. The reduction of the mobility due to heating
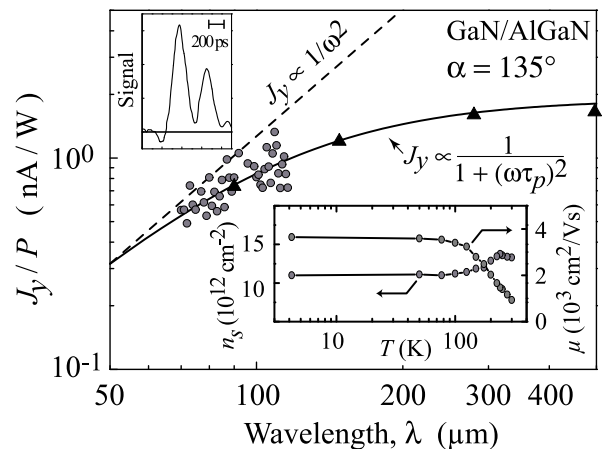

FIG. 3: Spectral dependence of the transverse photocurrent J_y measured at room temperature at oblique incidence ($\theta_0 = 15°$) for azimuth angle $\alpha = 135°$. The data are obtained with the free electron laser FELIX (dots) and with molecular optically pumped laser (triangles). Full line shows fit to Eq. (1). The fit is obtained using τ_p as an adjustable parameter and a scaling the whole dependence by the ordinate. Dashed line shows $J_y \propto \omega^{-2}$ for comparison. The inset in the left upper corner shows the temporal structure of the current in response to the radiation of FELIX. The inset in the right corner shows the temperature dependences of the carrier density and the mobility.

stems from enhancement of scattering by phonons under increase of temperature. Using short 6 ps pulses of FELIX we observed that the response time is determined by the time resolution of our set-up but it is at most 100 ps or shorter (see the inset in the left upper corner of Fig. 3). This fast response is typical for photogalvanics where the signal decay time is expected to be of the order of the momentum relaxation time[3,4,14] being in our samples at room temperature of the order of 0.1 ps.

In addition to the signal excited by the radiation at oblique incident we also detected a small photocurrent at normal incidence. The polarization behavior of this signal is shown in Fig. 4. In this set-up photocurrent dependences can be well fitted by $J_x = J_1 \sin 2\alpha$ and $J_y = J_1 \cos 2\alpha$ (see also Sec. IV.A). Rotating the sample around z axis we proved that the current direction is solely determined by the orientation of radiation electric field relative to the in-plane crystallographic axes. We note that this contribution is about one order of magnitude smaller than that at oblique incidence even at small angles $\theta_0 \approx 15°$.

Besides investigations of photocurrent in response to linearly polarized radiation we also performed measurements under excitation with elliptically polarized light. Such experiments are of particular interest because such radiation, in partially circularly polarized light, has previously been used for investigation of the circular photogalvanic effect (CPGE)[4,7,14] which coexist with the LPGE yielding beatings in φ_p-dependence. The CPGE is characterized by a photocurrent whose direction is
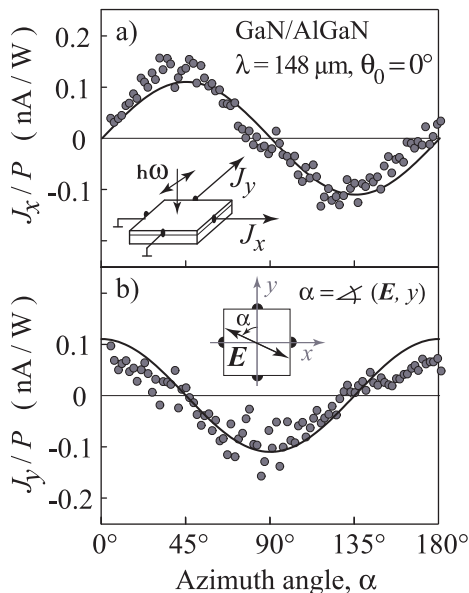
FIG. 4: Photocurrent as a function of angle α measured at normal incidence ($\theta_0 = 0$) in a) x and b) y crystallographic directions. Photocurrent is excited by linearly polarized radiation with wavelength $\lambda = 148$ μm and power $P \approx 5$ kW. Full lines are fits to Eqs. (5). To get agreement with experiments we used one fitting parameter $J_1 \propto \chi'$. The inset shows the experimental geometry. An additional inset in the lower panel displays the sample and the radiation electric field viewing from the source of radiation side.

changed upon reversal of the radiation helicity. It has been observed in GaN-based structures demonstrating a substantial structural inversion asymmetry (SIA) in this wide band gap material.[7,9,10,11] We have shown that SIA in GaN-based heterostructures results in a spin splitting of subbands in $\boldsymbol{k}$-space which was later confirmed by magneto-transport measurements.[18,19,20,21] The Rashba spin-splitting due to SIA, which is not expected in wide band semiconductors, in GaN/AlGaN heterostructures is caused by a large piezoelectric effect[22] which yields a strong electric field at the GaN/AlGaN interface and a strong polarization induced doping effect.[23]

Figures 5(a) and 5(b) demonstrate the dependences of the photocurrent on the angle φ_p for positive angle θ_0. In Fig. 5(a) transverse and longitudinal photocurrents are measured for the experimental set-up with $\boldsymbol{E}_l$ perpendicular to the incidence plane (s-polarization at $\varphi_p = 0$). We find that the polarization dependences in this experiment are well fitted by $J_x = J_0(1 - \cos 4\varphi_p)/2 + J_{\text{offset}}$ and for transverse geometry by $J_y = -J_0 \sin 4\varphi_p /2 + J_2 \sin 2\varphi_p$, see Sec. IV.B.2 for theoretical justification. We note that we used for fitting the same values of J_0 and J_{offset} as in experiments with linearly polarized radiation.

As we discussed above our laser can generate linearly polarized radiation either oriented along or perpendicularly to the polarization of the pump radiation. By that we change the position of the electric field of transformed beam relative to the optical axis of the quarter-wave plate, consequently changing the orientation of the ellipse as well as radiation helicity of the beam at the sample. In order to check how this transformation influence results we provided an additional experiment using laser beam with again $\lambda = 148$ μm and $\hat{\boldsymbol{e}}_\parallel \parallel x$ but for $\boldsymbol{E}_l$ parallel to the incidence plane (p-polarization at $\varphi_p = 0$). Figures 5(c),(d) show the data obtained in this geometry. In contrast to the results presented in Figs. 5(a),(b) the photocurrent now shows another type of polarization dependences: $J_x = J_0(3 + \cos 4\varphi_p)/2 + J_{\text{offset}}$ and for transverse geometry by $J_y = J_0 \sin 4\varphi_p/2 + J_2 \sin 2\varphi_p$. The fact that contribution given by J_2 did not change is not surprising because this term is due to radiation helicity which does not change: $P_{\text{circ}} = -\sin 2\varphi_p$. The changes in contribution induced by the degree of linear polarization are caused by the fact that the orientation of corresponding ellipses at the sample at a given φ_p is different.

The photocurrent polarization properties revealed experimentally both under normal and oblique incidence are explained in the next Section where we propose a simple illustrative model to interpret the nature of the photocurrent under study and derive general phenomenological equations. The measured wavelength and temperature dependences of the LPGE current are described in Sec. V where a microscopic theory is developed.

IV. MODELS, PHENOMENOLOGY AND POLARIZATION DEPENDENCES OF THE PHOTOCURRENTS

The appearance of the LPGE can be visualized by a simple one-dimensional model of randomly distributed but identically oriented wedges acting as asymmetric scattering centers.[3,4,14] This model showing the generation of a photogalvanic current is relevant for 2D GaN/AlGaN structures excited by the radiation at normal incidence. In Fig. 6 a wedge with a base oriented along x-direction is depicted which obviously does not possess a center of inversion. In equilibrium the velocities of electrons are isotropically distributed. Application of an external in-plane alternating field $\boldsymbol{E}(t) = \boldsymbol{E} \sin \omega t$ adds an oscillatory motion along the electric field to the random thermal motion of the electrons. If the field points along the height of the wedges ($\boldsymbol{E} \parallel y$, or $\alpha = 0$), then the scattering results in a carrier flow in the $(-y)$ direction yielding an electric current $j_y > 0$ shown by up-arrow in Fig. 6(a). By that electron fluxes along x direction compensate each other and j_x is absent. A variation of the relative direction between the electric field and the orientation of the wedges changes the direction of the carrier flow resulting in a characteristic polarization dependence. It may, e.g., reverse its direction, as it is shown in Fig. 6(b) for the field oriented along the base of the wedges, or rotate by $90°$ in the case of $\boldsymbol{E}$ directed at $45°$ to y axis.

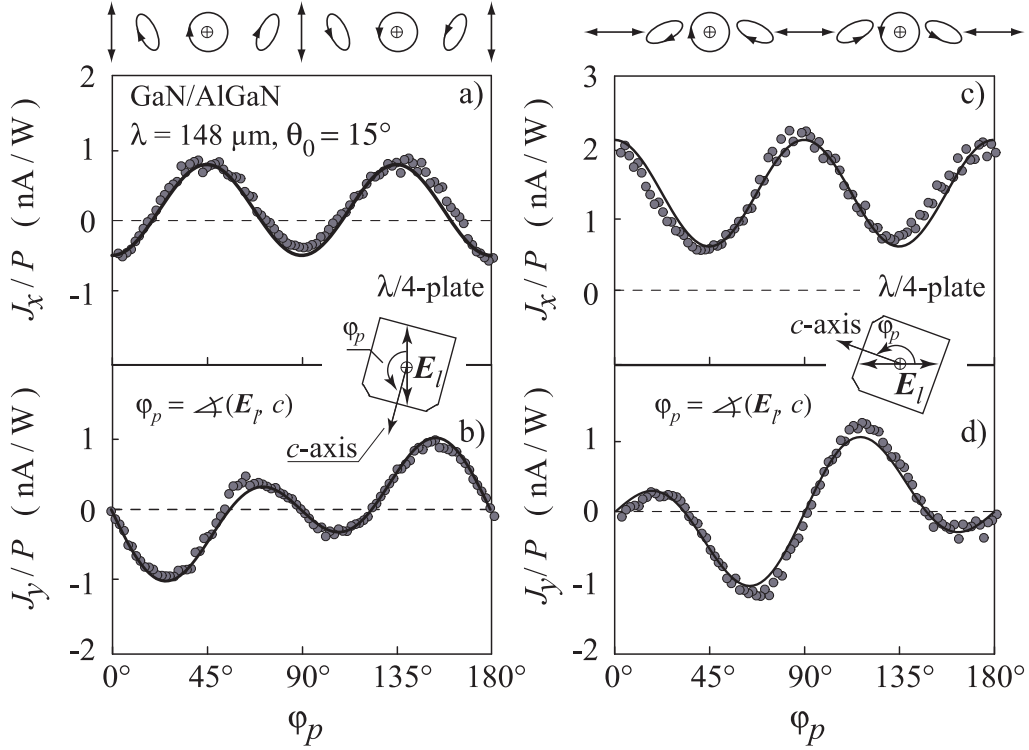In order to describe the observed polarization and an-

FIG. 5: Photocurrent as a function of angle φ_p measured at oblique incidence ($\theta_0 = 15°$) in the longitudinal [J_x in a) and c)] and transverse [J_y in b) and d)] geometries at wavelength $\lambda = 148$ μm and power $P \approx 5$ kW. The ellipticity of the radiation is varied by passing linearly polarized laser radiation ($\boldsymbol{E}_l$) through a quarter-wave plate (see insets in the left and right panels). Left panels show transverse and longitudinal photocurrents measured in experimental set-up with $\boldsymbol{E}_l$ perpendicular to the incidence plane (s-polarization at $\varphi_p = 0$, see inset in the left panel). Photocurrents obtained for $\boldsymbol{E}_l$ parallel to the incidence plane (p-polarization at $\varphi_p = 0$, see inset in the right panel) are shown in the right panel. Full lines are fits of the photocurrent to Eqs. (9) and (10) obtained correspondingly in the experimental set-up sketched in the inset in the left and right panels. The fits are obtained using the same values of J_0 and J_{offset} as in the experiments with linearly polarized radiation. The inset in the left panels shows the experimental geometry. On top the polarization ellipses corresponding to various phase angles φ_p are plotted viewing from the source of radiation.

gle of incidence dependences, we derive here phenomenological equations for the photocurrents in 2D GaN-based structures and give a model for LPGE. The linear photogalvanic current density $\boldsymbol{j}$ is phenomenologically described by the following expression[3,4,14]

$$j_\lambda^{LPGE} = \sum_{\mu\nu} \chi_{\lambda\mu\nu}(E_\mu E_\nu^* + E_\nu E_\mu^*) . \quad (2)$$

Here $\boldsymbol{E}$ is the electric field amplitude of the light wave, and $\boldsymbol{\chi}$ the third-rank tensor symmetric in the last two indices. The index λ enumerates two in-plane coordinates x and y, while μ and ν run over all three Cartesian coordinates.

The LPGE is allowed only in piezoelectric crystal classes of noncentrosymmetric media where nonzero components of the tensor $\boldsymbol{\chi}$ do exist. The point symmetry of wurtzite 2D electron systems confined in the [0001] direction is C$_{3v}$ which differs from the C$_{6v}$ symmetry of the bulk GaN due to absence of translation along the growth axis z, i.e., because of presence of interfaces. The coordinate frame x, y, z chosen in the experimental set-up means that the plane $(yz) \parallel (1\bar{1}00)$ coincides with the

mirror reflection planes σ_v contained in the C$_{3v}$ point group. In this point group the tensor $\boldsymbol{\chi}$ has two linearly-independent components for $\lambda \neq z$:

$$\chi \equiv \chi_{xxz} = \chi_{yyz}, \qquad \chi' \equiv \chi_{xxy} = \chi_{yxx} = -\chi_{yyy} . \quad (3)$$

This means that the phenomenological equation (2) reduces to

$$\begin{aligned} j_x^{LPGE} &= \chi\{E_x E_z^*\} + \chi'\{E_x E_y^*\}, \\ j_y^{LPGE} &= \chi\{E_y E_z^*\} + \chi'(|E_x|^2 - |E_y|^2) , \end{aligned} \quad (4)$$

where $\{E_\mu E_\nu^*\} = E_\mu E_\nu^* + E_\nu E_\mu^*$.

A. Normal incidence

In our experiments, a linear photogalvanic current is observed at normal incidence, see Fig. 4. It follows from Eqs. (4) that while at normal incidence the photocurrent proportional to the constant χ vanishes, because $E_z = 0$, the contribution determined by the constant
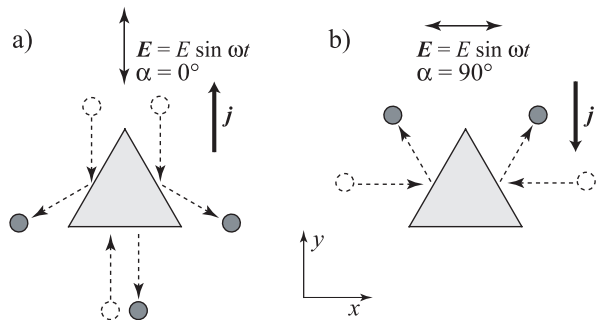
FIG. 6: Model of current generation due to asymmetry of specular elastic scattering by wedges. The field $\boldsymbol{E}$ results in directed motion of carriers shown by dashed arrows. Due to asymmetric scattering a directed carrier flow and, therefore, electric current $\boldsymbol{j}$ are generated. a) and b) sketch two relative orientations of wedges and the electric field $\boldsymbol{E}$ together with resulting dc current $\boldsymbol{j}$.

χ' is nonzero. The observation of this photocurrent is an important result demonstrating substantial difference in symmetry between wurtzite 2D GaN(0001)-based structures with C_{3v} symmetry and zinc-blende GaAs- and InAs-based heterostructures having C_{2v} or D_{2d} symmetry, where the LPGE is forbidden at normal light incidence.

The polarization dependences for normal incidence follow from Eqs. (4) and are given by

$$j_x = \chi'(t_0 E_0)^2 \sin 2\alpha \,, \qquad (5)$$
$$j_y = \chi'(t_0 E_0)^2 \cos 2\alpha \,,$$

where $t_0 = 2/(n_\omega + 1)$ is the amplitude transmission coefficient for normal incidence, n_ω is the refractive index of the medium (for GaN $n_\omega = 2.3$). Both polarization dependences well describe our experimental data with one fitting parameter χ' (see solid lines in Fig. 4). This agreement clearly demonstrates the generation of LPGE current at normal incidence. We emphasize that the current direction depends on the orientation of the polarization plane in respect to the crystallographic axes x and y. In the case that contacts are arbitrary oriented relative to the crystallographic directions Eqs. (5) hold but the phase shift appears. This is considered in Appendix A.

B. Oblique incidence

1. Linear polarization

Linear photogalvanic effect is also observed at oblique incidence. Moreover, comparison of Figs. 1 and 4 shows that even at a small incidence angle θ_0 the photocurrent is substantially (by the order of magnitude) larger than that at normal incidence. While at normal incidence the photogalvanic current is solely described by the constant χ' at oblique incidence another term in Eqs. (4) shows

up. This term is determined by the second linearly independent constant χ. The polarization dependence of this contribution in the geometry relevant to the experiment depicted in Fig. 1, where the incidence plane is chosen to be the plane (xz) and the angle α is counted from y, is given by

$$j_x(\alpha) = \chi E_0^2 t_p^2 \cos\theta \sin\theta (1 - \cos 2\alpha) \,, \qquad (6)$$
$$j_y(\alpha) = -\chi E_0^2 t_p t_s \sin\theta \sin 2\alpha \,.$$

Here θ is the refraction angle related to the incidence angle θ_0 by $\sin\theta = \sin\theta_0/n_\omega$, and t_s and t_p are the Fresnel amplitude transmission coefficients from vacuum to the structure for the s- and p-polarized light, respectively.[24] These functions are shown in Fig. 1 by solid lines. To get agreement with experiments we used the above equations with one fitting parameter χ and introduced an offset for the current J_x detected in the direction of the light propagation. Registration of these characteristic polarization dependences proves observation of LPGE at oblique incidence.

Comparing the results presented in Figs. 1 and 4 we can estimate of the ratio of different components of the tensor $\boldsymbol{\chi}$ for the studied structures. At $\theta \approx 0.1$ rad, $t_s \approx t_p \approx t_0$, therefore from the ratio of the amplitudes in Figs. 1 and 4 equal to $|\chi'/\chi\,\theta|$ we get $|\chi'/\chi| \approx 10^{-2}$. This hierarchy of components of the third rank tensor $\chi_{\lambda\mu\nu}$ in the systems of C_{3v} symmetry is expectable,[3] however we demonstrate that the χ'-related effect is observable. While the effect described by the constant χ also exists in the bulk GaN as well as in the $C_{\infty v}$ group the photocurrent proportional to χ' arises only due to the reduced symmetry C_{3v} of the system, i.e. due to size quantization. Therefore the latter contribution should increase at narrowing of 2D layer.

Equations (6) show that the photogalvanic current should follow the dependence $t_s t_p \sin\theta$, in particular, reverse its direction upon inversion the angle of incidence. This behavior is indeed observed. Figure 2 shows LPGE current dependence on the incidence angle, θ_0 obtained for J_y at a fixed linear polarization of radiation ($\alpha = 45°$). We note that the offset photocurrent observed in the longitudinal direction only is always directed antiparallel to $\hat{e}_\parallel$. We ascribe the offset to the photon drag current which is linearly coupled to the photon momentum. This effect is out of scope of the present paper.

In our experiments we also probe LPGE for the light directed along other crystallographic directions. Investigating transverse and longitudinal currents being perpendicular and parallel to the incidence plane, respectively, we observed that all polarization dependences are described by the same constant χ independently of the in-plane direction of the light propagation. The reason of this fact is that the current contribution proportional to χ is due to cone asymmetry being axial isotropic in the plane of our structures. Thus this photocurrent is totally determined by the light polarization state and propagation direction, and it is independent of the incidence

plane orientation relative to the in-plane crystallographic axes. For linearly polarized light the photocurrent can be presented in the invariant form as $\boldsymbol{j} = 2\chi \boldsymbol{E}_\parallel E_z$ where $\boldsymbol{E}_\parallel$ is the projection of the light polarization vector $\boldsymbol{E}$ onto the structure plane. It is seen that the LPGE current is always directed along $\boldsymbol{E}_\parallel$. By introducing the azimuth angle β so that $\beta = 0$ corresponds to the polarization perpendicular to the incidence plane (s-polarization) we obtain for transverse ($\boldsymbol{j}_\perp$) and longitudinal ($\boldsymbol{j}_\parallel$) currents

$$\boldsymbol{j}_\perp = \chi E_0^2 t_p t_s \sin 2\beta \, (\hat{\boldsymbol{e}}_\parallel \times \hat{\boldsymbol{z}}) \,, \tag{7}$$

$$\boldsymbol{j}_\parallel = \chi E_0^2 t_p^2 \cos \theta \, (1 - \cos 2\beta)\hat{\boldsymbol{e}}_\parallel \,,$$

where $\hat{\boldsymbol{z}}$ is the unit vector along the normal.

2. Elliptical polarization

Illumination of the structure by elliptically polarized radiation also results in generation of the LPGE current which is determined by the linear polarization degree of the light. However, elliptically polarized radiation is also characterized by the nonzero helicity. This results in the additional effect solely determined by the degree of circular polarization, the circular photogalvanic effect.[3,4,14] This effect is phenomenologically described by

$$j_\lambda^{CPGE} = \sum_\mu \gamma_{\lambda\mu} \, \mathrm{i}(\boldsymbol{E} \times \boldsymbol{E}^*)_\mu = E_0^2 t_p t_s P_{circ}(\boldsymbol{\gamma}\hat{\boldsymbol{e}})_\lambda \,, \tag{8}$$

where $\hat{\boldsymbol{e}}$ is the light propagation unit vector and $\boldsymbol{\gamma}$ the second-rank pseudotensor. In the systems of C_{3v} symmetry the tensor $\boldsymbol{\gamma}$ has one linearly-independent component, namely $\gamma_{xy} = -\gamma_{yx} \equiv \gamma$. Thus, the CPGE current flows always perpendicularly to the incidence plane.

In our experimental set-up a quarter-wave plate is rotated by the angle φ_p between the laser light polarization vector, $\boldsymbol{E}_l$, and the principal axis of the polarizer (see inset to Fig. 5). The total photogalvanic current is given by both second and fourth harmonics of this angle. While radiation handedness is solely determined by the angle φ_p and does not depend on the relative orientation between $\boldsymbol{E}_l$ and the plane of incidence the orientation of the ellipse is substantially different. In particular, for $\boldsymbol{E}_l$ perpendicular to the incidence plane at $\varphi_p = 0$ (s-polarization) and for $\boldsymbol{E}_l$ parallel to the incidence plane at $\varphi_p = 0$ (p-polarization) the orientation of corresponding ellipses on the sample differs by 90°. Therefore in the former case light is never p-polarized and in the latter case s-polarization can not be achieved, which is quite different from the geometry of half-wave plate where all states of linear polarization can be obtained. Thus we derive two sets of equations describing experimental set-up of Figs. 5(a),(b) and 5(c),(d).

In the first geometry (s-polarization at $\varphi_p = 0$) from Eqs. (4) and (8) we get

$$j_x(\varphi_p) = \frac{\chi}{2} E_0^2 t_p^2 \cos \theta \sin \theta \, (1 - \cos 4\varphi_p) \,, \tag{9}$$

$$j_y(\varphi_p) = E_0^2 t_p t_s \sin \theta \, \left(-\frac{\chi}{2} \sin 4\varphi_p + \gamma \sin 2\varphi_p\right) \,,$$

and for the latter geometry (p-polarization at $\varphi_p = 0$)

$$j_x(\varphi_p) = \frac{\chi}{2} E_0^2 t_p^2 \cos \theta \sin \theta \, (3 + \cos 4\varphi_p) \,, \tag{10}$$

$$j_y(\varphi_p) = E_0^2 t_p t_s \sin \theta \, \left(\frac{\chi}{2} \sin 4\varphi_p + \gamma \sin 2\varphi_p\right) \,.$$

Here we again took into account that in our samples $|\chi'| \ll |\chi|$. Fits of experiment with the constant χ independently obtained from experiments with half-wave plates and γ as a single adjustable parameter being the same for all curves yields a good agreement with the experiment. Here again for the longitudinal photocurrent the offset due to photon drag effect shows up and has the same value as that in the experiments with half-wave plates.

V. MICROSCOPIC THEORY

In order to describe the measured dependences of the photocurrent on wavelength and temperature we have developed a microscopic theory of LPGE. First we consider the contribution proportional to the coefficient χ in Eqs. (4). This contribution does exist not only in systems of the C_{3v} or C_{6v} symmetry but is also allowed by the uniaxial point group $C_{\infty v}$. Therefore, we can calculate the χ contribution to $j_{x,y}^{\text{LPGE}}$ in the uniaxial approximation. Then we turn to calculation of the contribution proportional to χ' in Eqs. (4) and surviving under normal incidence due to the reduced C_{3v} symmetry of the system. We note, that so far the LPGE in 2D systems has been treated theoretically for direct intersubband transitions only.[25,26] The mechanism of the LPGE under Drude absorption differs strongly because scattering is unavoidably present in the intrasubband absorption process.

A. Microscopic model for oblique incidence

Microscopically the LPGE current consists of the shift and ballistic contributions which in general can be comparable in order of magnitude. We start from the analysis of the shift contribution and then turn to the ballistic contribution.

1. Shift contribution

The shift contribution arises due to coordinate shifts of the free-carrier wave-packet center-of-mass by microscopic lengths in quantum transitions. The corresponding current is a product of the elementary charge e, the transition probability rate $W_{\boldsymbol{k}'\boldsymbol{k}}$ and the shift vector $\boldsymbol{R}_{\boldsymbol{k}'\boldsymbol{k}}$ or, explicitly,

$$\boldsymbol{j}_{\text{LPGE}}^{(\text{shift})} = 2e \sum_{\boldsymbol{k},\boldsymbol{k}'} W_{\boldsymbol{k}'\boldsymbol{k}} \, \boldsymbol{R}_{\boldsymbol{k}'\boldsymbol{k}} \,, \tag{11}$$

where the factor "two" accounts for spin degeneracy. The elementary shift is related to the transition matrix element $M_{\boldsymbol{k'k}}$ by[5]

$$\boldsymbol{R}_{\boldsymbol{k'k}} = -\frac{\text{Im}[M_{\boldsymbol{k'k}}^*(\nabla_{\boldsymbol{k}} + \nabla_{\boldsymbol{k'}})M_{\boldsymbol{k'k}}]}{|M_{\boldsymbol{k'k}}|^2} \qquad (12)$$
$$= -(\nabla_{\boldsymbol{k}} + \nabla_{\boldsymbol{k'}})\arg(M_{\boldsymbol{k'k}}),$$

where $\arg(u)$ is the phase of the complex number u. The above two equations are general and valid for the shift photocurrent calculation in any frequency range.[3,4] Here, for the first time, we apply them to consider the LPGE under the Drude absorption. Note that Eq. (12) was applied in the theory of anomalous Hall effect[6,27] where the coordinate shift at scattering is called a side-jump.

The main contribution to the matrix element for indirect intrasubband optical transitions,

$$M_{1\boldsymbol{k'},1\boldsymbol{k}}^{\parallel} = U_{1\boldsymbol{k'},1\boldsymbol{k}}\left(\frac{V_{\boldsymbol{k'}}}{E_{\boldsymbol{k'}} - E_{\boldsymbol{k}}} - \frac{V_{\boldsymbol{k}}}{\hbar\omega}\right), \qquad (13)$$

comes from two-quantum processes a_1 and a_2 with intermediate virtual states in the same $e1$ subband, see Fig. 7. Here the 2D electron kinetic energy $E_{\boldsymbol{k}} = \hbar^2 k^2/2m$, m
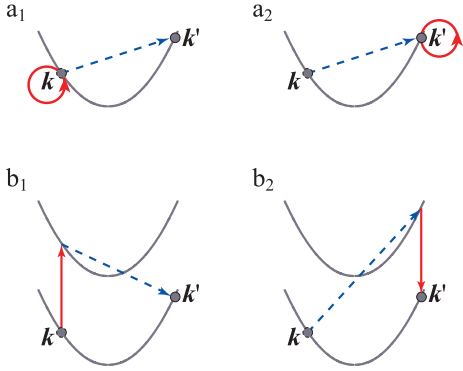

FIG. 7: The quantum transitions responsible for the shift contribution to the photocurrent. Note that Drude absorption under oblique light incidence is caused by a_1 and a_2 processes only.

is the electron in-plane effective mass, $V_{\boldsymbol{k}}$ is the matrix element of electron-light interaction

$$V_{\boldsymbol{k}} = -\frac{e\hbar A}{mc}\,\boldsymbol{e}\cdot\boldsymbol{k},$$

ω, A and $\boldsymbol{e}$ are the frequency, amplitude and unit polarization vector of the light wave, $U_{1\boldsymbol{k'},1\boldsymbol{k}}$ is the matrix element of intrasubband elastic scattering $e1, \boldsymbol{k} \to e1, \boldsymbol{k'}$, the superscript $\parallel$ indicates that the process is allowed for the polarization $\boldsymbol{e}$ containing an in-plane component $\boldsymbol{e}_{\parallel}$. In the following, for simplicity, we ignore the wave vector dependence of $U_{1\boldsymbol{k'},1\boldsymbol{k}}$ and replace it by a constant U_{11}. The probability rate $W_{\boldsymbol{k'k}}$ is given by Fermi's golden rule and expressed via the squared modulus of the transition matrix element and δ-function describing the energy conservation

$$E_{\boldsymbol{k'}} - E_{\boldsymbol{k}} = \hbar\omega. \qquad (14)$$

The processes a_1 and a_2 in isolation from other processes make no contribution to $\boldsymbol{j}_{\text{LPGE}}^{(\text{shift})}$, because $M_{1\boldsymbol{k'},1\boldsymbol{k}}^{\parallel}$ is independent of e_z while the χ-related photocurrent in the phenomenological equations (4) is proportional to e_z, or because the microscopic expression in the square brackets in Eq. (12) is real and hence the elementary shift is absent. The shift contribution becomes nonzero if two other indirect processes, b_1 and b_2 in Fig. 7, are taken into account. The virtual states in these processes lie in the second size-quantized subband $e2$. The corresponding matrix element reads as

$$M_{1\boldsymbol{k'},1\boldsymbol{k}}^{\perp} = -\text{i}e_z\frac{eA}{\hbar c}z_{21}\Delta_{21}\left(\frac{U_{12}}{\Delta_{21} - \hbar\omega} - \frac{U_{21}}{\Delta_{21} + E_{\boldsymbol{k'}} - E_{\boldsymbol{k}}}\right). \qquad (15)$$

Here $U_{21} = U_{12}$ is the intersubband scattering matrix element, Δ_{21} is the energy spacing between the $e2$ and $e1$ subbands, and z_{21} is the intersubband matrix element of the coordinate z. The superscript $\perp$ indicates that the transitions (15) are allowed in the polarization perpendicular to the interface plane.

Substituting $M_{\boldsymbol{k'k}} = M_{\boldsymbol{k'k}}^{\parallel} + M_{\boldsymbol{k'k}}^{\perp}$ into Eq. (12), taking then into account the energy conservation equation (14) and assuming $\hbar\omega \ll \Delta_{21}$ we obtain for the elementary shift

$$|M_{\boldsymbol{k'k}}|^2\,\boldsymbol{R}_{\boldsymbol{k'k}} \qquad (16)$$
$$= -z_{21}\left(\frac{e\hbar A}{mc}\right)^2\frac{U_{11}U_{21}}{\Delta_{21}\hbar\omega}e_z[\boldsymbol{e}\cdot(3\boldsymbol{k'} - \boldsymbol{k})]\,(\boldsymbol{k'} - \boldsymbol{k}).$$

Note that the shift is different from zero only due to the wave vector dependence of denominators $E_{\boldsymbol{k'}} - E_{\boldsymbol{k}}$ and $\Delta_{21} + E_{\boldsymbol{k'}} - E_{\boldsymbol{k}}$ in the matrix elements (13) and (15).

The result for the shift photocurrent can be presented in the form

$$\boldsymbol{j}_{\text{LPGE}}^{(\text{shift})} = -e\xi z_{21}\boldsymbol{e}_{\parallel}e_z\frac{\eta_{\parallel}I}{\Delta_{21}}\frac{F[4E + 3\hbar\omega]}{F[2E + \hbar\omega]}. \qquad (17)$$

Here the factor ξ is given by[28]

$$\xi = \frac{\langle U_{11}U_{21}\rangle}{\langle U_{11}^2\rangle},$$

where the angular brackets mean averaging over the distribution of static scatterers along z, the functional $F[\phi(E)]$ turns any function $\phi(E)$ into a real number as follows

$$F[\phi(E)] = \int_0^\infty [f(E) - f(E + \hbar\omega)]\phi(E)dE \left/ \int_0^\infty f(E)dE \right. ,$$

$f(E)$ is the Fermi-Dirac distribution function, $\eta_{\parallel}$ is the absorbance under normal incidence ($\theta = 0$) given by[29]

$$\eta_{\parallel} = \frac{e^2}{\hbar c}\frac{2\pi N_s}{n_\omega m\omega^3\tau_p}\,F[2E + \hbar\omega], \qquad (18)$$

the momentum relaxation time $\tau_p = \hbar^3/(mN_d\langle U_{11}^2\rangle)$, N_s and N_d are the 2D concentrations of electrons and scatterers.

Note that allowance for nonzero value of ξ and, hence, of the LPGE current, presupposes the uniaxial asymmetry of the structure.[28] This corresponds to phenomenology of the LPGE which requires absence of an inversion center in the system. A value of ξ is nonzero due to an asymmetrical shape of the electron envelope functions in the $e1$ and $e2$ subbands caused by the build-in electric field. An inhomogeneous asymmetrical distribution of scatterers along the z axis can also contribute to ξ.

2. Ballistic contribution

In order to obtain a nonzero ballistic photocurrent it is necessary to go beyond the approximation of single-impurity scattering and take into account simultaneous scattering by two impurities in one process. Such optical-absorption processes are schematically shown in Fig. 8. Let us introduce the antisymmetrical part, $W_{k'k}^a$, of the $k \to k'$ transition rate $W_{k'k}$ which changes sign under simultaneous inversion of the wave vectors k and k'. It can be expressed in terms of Fermi's golden rule

$$W_{k'k}^a = \frac{2\pi}{\hbar}\,|M_{k'k}|_a^2\,[f(E_k) - f(E_{k'})]\,\delta(E_{k'} - E_k - \hbar\omega)\,,$$
(19)

where $|M_{k'k}|_a^2$ is the antisymmetric part of the squared modulus of the optical two-impurity-mediated matrix element $M_{k'k}$. Then the ballistic contribution to the LPGE current is given by

$$j_{\mathrm{LPGE}}^{(\mathrm{ball})} = 2e\sum_{k,k'} W_{k'k}^a\,\tau_p\,(v_{k'} - v_k)\,,$$
(20)

where $v_k = \hbar k/m$ is the electron velocity.

Here it is worth to discuss the dependence of the ballistic and shift contributions on the concentration of elastic scatterers N_d. For two-impurity scattering the probability rate $W_{k'k}^a \propto N_d^2$. In contrast, the single-impurity scattering rate $W_{k'k}$ in Eq. (11) linearly depends on N_d. However, the ballistic current is controlled by the momentum relaxation time, see the factor τ_p in the right-hand side of Eq. (20). Since $\tau_p \propto N_d^{-1}$, the ballistic and shift currents are both proportional to N_d. In this sense, there is an analogy between a pair of the two contributions to the photocurrent and a pair of the side-jump and skew-scattering currents in the anomalous Hall effect.[6]

In order to get the photocurrent proportional to both $e_\parallel$ and e_z, we extract from $|M_{k'k}|^2$ the interference term proportional to $\mathrm{Re}\{M^\parallel M^{\perp*}\}$, where $M^\parallel$ and $M^\perp$ are the contributions to the matrix element of the indirect optical transition proportional to $e_{x,y}$ and e_z, respectively. To the lowest order in $\hbar\omega/\Delta_{21} \ll 1$, one should include into consideration six two-impurity scattering processes $a_3\ldots a_8$ contributing to $M^\parallel$ and two processes b_3, b_4 for $M^\perp$ depicted in Fig. 8.

For example, below we present the contributions to $M^\parallel$ from the processes a_5 and a_6,

$$M_{a_5}^\parallel = N_d \times$$
(21)
$$\sum_{k_1 k_2} \frac{U_{11}'\,V_{k_2}\,U_{11}\,U_{11}'\,\delta_{k+k_2,k'+k_1}}{(E_{k_2} - E_k - \hbar\omega - \mathrm{i}0)(E_{k_2} - E_k - \mathrm{i}0)(E_{k_1} - E_k - \mathrm{i}0)},$$

$$M_{a_6}^\parallel = N_d \times$$
$$\sum_{k_1 k_2} \frac{V_{k'}\,U_{11}'\,U_{11}\,U_{11}'\,\delta_{k+k_2,k'+k_1}}{(E_{k'} - E_k - \mathrm{i}0)(E_{k_2} - E_k - \mathrm{i}0)(E_{k_1} - E_k - \mathrm{i}0)},$$

where the prime means the scattering (shown by dotted lines in Fig. 8) by a defect different from that which is related to the matrix element U_{11} in these equations and to U_{21} in Eq. (15) (shown by dashed lines). The Kronecker symbols are obtained after averaging the matrix element over the in-plane distribution of the second scatterer. Note that averaging over its distribution in the z direction results in replacement of the square $(U_{11}')^2$ by $\langle U_{11}^2\rangle$. The energy denominators are rewritten by using the identity

$$\frac{1}{x - \mathrm{i}0} = PV\frac{1}{x} + \mathrm{i}\pi\delta(x)\,,$$

and, among three such terms in each contribution $M_{a_j}^\parallel$ ($j = 3...8$), we retain the δ-function in one of them and take the Cauchy principal values for two others. This additional δ-function, together with the energy conservation law (14) and the relation $k + k_2 = k' + k_1$, fixes absolute values of the wave vectors k, k', k_1 and k_2. The integration over the azimuthal angle of the vector k_1 either k_2 is performed by using the principal value integral

$$PV\int_0^{2\pi} \frac{d\varphi}{2\pi}\frac{1}{a - b\cos\varphi} = \frac{\Theta(a^2 - b^2)\,\mathrm{sign}\,a}{\sqrt{a^2 - b^2}}\,,$$

where $\Theta(x)$ is the Heaviside step-function. The calculation shows that, among eight processes presented in Fig. 8, only two, namely, the processes a_5 and a_6, lead to nonzero ballistic current. The final result for this current reads

$$j_{\mathrm{LPGE}}^{(\mathrm{ball})} = e_\parallel e_z \frac{\eta_\parallel I}{\Delta_{21}}\xi e z_{21}\frac{F[L(\hbar\omega/E)]}{F[E/\hbar\omega + 1/2]}\,,$$
(22)

where

$$L(x) = \frac{x}{2\pi}\int_{\varphi_0(x)}^{2\pi} \frac{d\varphi}{\sqrt{(x - 2\sqrt{1+x}\cos\varphi)^2 - 4}}\,,$$

$$\varphi_0(x) = \Theta(8 - x)\arccos\left(\frac{x-2}{2\sqrt{1+x}}\right).$$
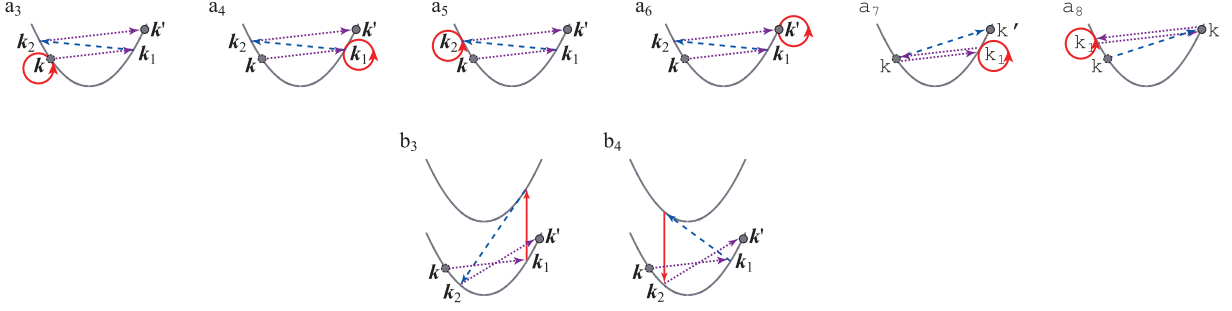
FIG. 8: Optical two-impurity-mediated processes included into consideration in order to obtain nonvanishing antisymmetric part of the scattering rate $W^a_{\bm{k}'\bm{k}}$ in Eq. (19). For the processes a$_{3\ldots6}$, the wave vectors satisfy the relation $\bm{k} + \bm{k}_2 = \bm{k}' + \bm{k}_1$.

The function $L(x)$ goes to zero as $x/4$ at $x \to 0$, and tends to 1 at $x \to \infty$. A sum of the shift and ballistic contributions given by Eqs. (17) and (20) represents the photocurrent phenomenologically described by the coefficient χ in Eqs. (4).

B. Microscopic model for normal incidence

An ideal GaN/AlN interface has the point-group symmetry C$_{3v}$ which is a subgroup of the C$^4_{6v}$ space group of a bulk wurtzite crystal. The group C$^4_{6v}$ is nonsymmorphic and contains, in addition to C_3 and σ_v, the elements $\{C_6|\bm{\tau}\}, \{\sigma_d|\bm{\tau}\}$, where $\bm{\tau}$ is the fractional lattice translation $(0,0,c/2)$ and c is the lattice constant along the principal axis z. In the 2D structures, the screw-axis and glide-plane operations shift the interfaces along z not bringing the system into coincidence with itself and, as a result, the point-group symmetry reduces to C$_{3v}$.

For the C$_{6v}$ symmetry of bulk wurtzite structure, characteristic of III-nitrides, the nonvanishing third order tensor components $\chi_{\lambda\mu\nu}$ symmetrical in μ and ν are χ_{zzz}, $\chi_{zxx} = \chi_{zyy}$, $\chi_{xxz} = \chi_{xzx} = \chi_{yyz} = \chi_{yzy} \equiv \chi$. Therefore, forbidden are such bulk effects as the second-harmonic generation for excitation along z, a piezoelectric field induced in the (x,y) plane under the deformation in this plane and the photocurrent in the (x,y) plane for the light propagating along z. The reduction from C$_{6v}$ to C$_{3v}$ removes these restrictions and four new nonzero components appear, $\chi_{xxy} = \chi_{xyx} = \chi_{yxx} = -\chi_{yyy} \equiv \chi'$, see Eqs. (4). Note that it is the interface that is exclusively responsible for the appearance of new components.

Here we propose a microscopic model of the LPGE under normal incidence. In this geometry virtual transitions via other size-quantized electronic subbands are forbidden, therefore we should consider the light absorption with intermediate states either in the same $e1$ electronic subband or in the valence band. In the first case, see Fig. 7, the reduced C$_{3v}$ symmetry manifests itself in the scattering matrix element $U_{1\bm{k}',1\bm{k}}$, and, instead of Eq. (16), one should replace the elementary shift in the

product $|M_{\bm{k}'\bm{k}}|^2 \bm{R}_{\bm{k}'\bm{k}}$ by the scattering induced shift

$$\bm{R}^{(U)}_{\bm{k}'\bm{k}} = -\frac{\mathrm{Im}[U^*_{1\bm{k}',1\bm{k}}(\nabla_{\bm{k}} + \nabla_{\bm{k}'})U_{1\bm{k}',1\bm{k}}]}{|U_{1\bm{k}',1\bm{k}}|^2} .$$

Note that the main contribution to $U_{1\bm{k}',1\bm{k}}$ dependent only on the difference $(\bm{k}' - \bm{k})$ does not result in the shift because the operator $(\nabla_{\bm{k}} + \nabla_{\bm{k}'})$ nullifies such a term. Similar contribution to the LPGE current has been calculated for Drude absorption in the heavy-hole subband of a bulk p-GaAs,[30] where the shift appeared due to interference of polar and deformation scattering mechanisms on optical phonons.

For optical transitions going via Γ_6 valence-band states, the elementary shift can be related to asymmetry of the interband optical matrix elements in which case the asymmetry of the interband scattering matrix element is neglected. We consider this mechanism in more detail. Taking into account the symmetry considerations we can present the interband matrix elements of the operator $\bm{e}_\parallel \cdot \bm{p}$ ($\bm{p}$ is the momentum operator) between the conduction-band state Γ_1 and the valence-band states Γ_6 as

$$\bm{e}_\parallel \cdot \bm{p}_{c\Gamma_1;v,\Gamma_{6x}}(\bm{k}) = \mathrm{i}\mathcal{P}e_x + \mathcal{Q}(e_x k_y + e_y k_x) , \quad (23)$$
$$\bm{e}_\parallel \cdot \bm{p}_{c\Gamma_1;v,\Gamma_{6y}}(\bm{k}) = \mathrm{i}\mathcal{P}e_y + \mathcal{Q}(e_x k_x - e_y k_y) ,$$

where $\mathcal{P}$ and $\mathcal{Q}$ are real constants. Multi-band derivation of these contributions for GaN-based 2D structures is given in Appendix B. The matrix element $\mathcal{Q}$ is nonzero due to the presence of the interface in the heterostructure. This approach is similar to description of interface inversion asymmetry induced spin splitting in the envelope-function method where δ-functional terms are introduced into the interband Hamiltonian, see Refs. 31,32. As a result, we expect a strong dependence of $\mathcal{Q}$ on the confinement size because $\mathcal{Q}$ is proportional to a product of the electron and hole envelope functions at the interface, see Eq. (B3). We expand $M_{\bm{k}'\bm{k}}$ and $\bm{R}_{\bm{k}'\bm{k}}$ in powers of small parameters $\hbar\omega/E_g$, $\bar{E}/E_g \ll 1$. In the same nonvanishing order we should take into account k-dependence of the matrix element $\mathcal{P}$. This could be done

by replacing in Eq. (23) the constant $\mathcal{P}$ by the function

$$\mathcal{P}(\boldsymbol{k}) = \mathcal{P}_0 \left(1 - \frac{E_{\boldsymbol{k}}}{2E_g}\right) .$$

The interband scattering $c\Gamma_1 \boldsymbol{k} \leftrightarrow v\Gamma_{6x}\boldsymbol{k}'$ and $c\Gamma_1 \boldsymbol{k} \leftrightarrow v\Gamma_{6y}\boldsymbol{k}'$ is described by the constant matrix elements U_{cv_x} and U_{cv_y} assumed to be independent of $\boldsymbol{k}$ and $\boldsymbol{k}'$, with $\langle U_{cv_x}^2 \rangle = \langle U_{cv_y}^2 \rangle$.

In order to carry out a reasonable estimation of the coefficient χ' in Eqs. (4) we have used a simple nonrelativistic $\boldsymbol{k} \cdot \boldsymbol{p}$ model coupling the $c\Gamma_1$ and $v\Gamma_6$ band states. In this model the valence band consists of two subbands, one with an infinite in-plane effective mass and the other with the hole in-plane effective mass coinciding with that for a conduction-band electron. Omitting the details of derivation we present the final result

$$\chi' = \frac{2\pi e^3}{m_0^2 \omega} \frac{\langle U_{cv_x}^2 \rangle \mathcal{P}_0 \mathcal{Q}}{E_g^3} N_s F_1 , \qquad (24)$$

where $F_1 \equiv F[1] = \int_0^\infty [f(E) - f(E+\hbar\omega)]dE \Big/ \int_0^\infty f(E)dE$. Experiment shows a noticeable magnitude of the LPGE current under normal incidence, see Fig. 4.

VI. DISCUSSION

In this Section we discuss the role of the contributions to the total current and analyze the frequency and temperature dependences of LPGE. An analytical estimation for the shift and ballistic photocurrents at Drude absorption is readily available for the photon energies $\hbar\omega$ small as compared to the electron typical energy $\bar{E}$ which is relevant to our experiments performed at room temperature and applying THz radiation. In this case Eqs. (17) and (22) reduce to

$$j_{\mathrm{LPGE}}^{(\mathrm{shift})} \sim 2\xi e z_{21} \frac{\eta_\parallel I}{\Delta_{21}} ,$$

$$j_{\mathrm{LPGE}}^{(\mathrm{ball})} \sim \xi e z_{21} \frac{\eta_\parallel I}{\Delta_{21}} \left(\frac{\hbar\omega}{2\bar{E}}\right)^2 .$$

Since $\hbar\omega/\bar{E} \ll 1$ the shift contribution dominates the LPGE. This estimation is confirmed by the study of the frequency dependence of LPGE. Indeed, while the shift photocurrent follows the frequency dependence of the absorbance which, for Drude processes, is given by Eq. (1), the ballistic contribution has another frequency dependence because in this case $j_{\mathrm{LPGE}}^{(\mathrm{ball})} \propto \eta_\parallel \omega^2$. The observed good agreement of the current and absorption frequency behavior (see Fig. 3) unambiguously proves the dominating role of the shift contribution to the LPGE. We note, that such a spectral behavior of the LPGE has been previously observed in bulk III-V semiconductors.[33]

We note that even for the opposite limit of $\hbar\omega/\bar{E} \gg 1$ the LPGE due to Drude absorption is still dominated

by the shift contribution. In this case estimations yield $\boldsymbol{j}_{\mathrm{LPGE}}^{(\mathrm{shift})} = -(3/2)\boldsymbol{j}_{\mathrm{LPGE}}^{(\mathrm{ball})}$.

Now we analyze the temperature dependence. As follows from Eq. (17), the temperature dependence of the LPGE current is given by $j_{\mathrm{LPGE}}^{(\mathrm{shift})} \propto \xi \eta_\parallel(T)$. Taking into account temperature behavior of the Drude absorption [see Eq. (18)] we get $j_{\mathrm{LPGE}}^{(\mathrm{shift})} \propto \xi/\tau_p(T)$. Here we again use the relation $\hbar\omega \ll \bar{E} \sim k_{\mathrm{B}}T$. Variation of the temperature results in the change of the dominant scattering mechanisms. Typically in the low-dimensional structures by raising temperature we get a transition from the temperature-independent scattering rate by impurities $1/\tau_p^{imp}$ to the fast-increasing rate due to scattering by phonons $1/\tau_p^{ph}(T)$. As a result we have for the LPGE current

$$j_{\mathrm{LPGE}}^{(\mathrm{shift})} \propto \frac{\xi_{imp}}{\tau_p^{imp}} + \frac{\xi_{ph}}{\tau_p^{ph}(T)}.$$

This expression demonstrates that despite the inverse mobility $1/\mu(T) \propto 1/\tau_p^{imp} + 1/\tau_p^{ph}(T)$ is a monotonous function of temperature (see inset in Fig. 3) and the asymmetry factors ξ are temperature-independent, the LPGE current can have a minimum or even change the sign at temperature increase. This is due to the interplay between two contributions to the LPGE caused by different scattering mechanisms characterized by substantially different values of ξ_{imp} and ξ_{ph} possibly being even opposite in signs. Due to the fact that only one time is temperature dependent $[\tau_p^{ph}(T)]$ variation of temperature may result in the dominance of one or the other contribution to the LPGE current.

VII. CONCLUSION

In conclusion, we have studied the linear photogalvanic effect in wurtzite GaN(0001)-based heterojunctions under excitation by linearly and elliptically polarized light in the terahertz frequency range. Experimentally, the properties of LPGE have been revealed as a function of the incidence angle and the polarization state of radiation. A detailed point-group symmetry analysis of the polarization properties shows an agreement between the experiment data and the phenomenological theory of LPGE. Phenomenologically, the effect is described by two linearly independent coefficients χ and χ', the former being allowed by the C_{3v}, C_{6v} and even $C_{\infty v}$ symmetries and the latter being nonzero only for the C_{3v} symmetry. An observation of the photocurrent under normal incidence determined by χ' unambiguously demonstrates a reduction of the heterojunction symmetry from hexagonal C_{6v} to trigonal C_{3v}. However, beginning from very small oblique angles first contribution to the photocurrent prevails over the second one. The frequency dependence of the measured LPGE photocurrent exhibits a Drude-like behavior. A microscopic theory of LPGE under the intrasubband (Drude) absorption in the lowest

*e*1 electron subband has been developed. While calculating the χ-related photocurrent we have included virtual indirect optical transitions via the higher subband *e*2, estimated both the shift and ballistic contributions and showed that the first one exceeds the other by a large factor $\propto (\bar{E}/\hbar\omega)^2$. The dominating shift photocurrent repeats a Lorentzian frequency dependence of the Drude-absorption coefficient, in agreement with the experiment. The temperature dependence of the photocurrent is governed by a product of the absorption coefficient and the dimensionless parameter of asymmetry. Microscopically, the contribution nonvanishing under normal incidence arises taking into account indirect optical transitions via virtual electronic states in the valence band.
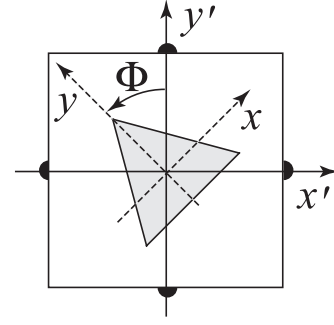

FIG. 9: Schematic representation of the orientation of the crystallographic axes x, y relative to the directions x', y' along which the current is measured.

APPENDIX A: PHOTOCURRENTS IN THE ROTATED COORDINATE FRAME

In the Section IV.A we get phenomenological equations for LPGE at normal incidence. We obtained that the photocurrent direction is determined by the orientation of the electric vector with respect to the crystallographic axes x and y. Most convenient for this effect is to investigate the current in the directions along and perpendicular to one of the mirror reflection planes of the C_{3v} point group. However, in contrast to III-V semiconductor heterostructures where well determined in-plane crystallographic orientation is naturally obtained by cleaving, in GaN/AlGaN heterojunctions grown on the sapphire substrate this may be not the case. Therefore we obtain here the LPGE for the arbitrary orientation of contacts in respect to the crystallographic directions. To describe this situation we introduce the angle Φ between the in-plane directions x' and y' along which the contacts are made and the crystallographic axes x and y, see Fig. 9. The symmetry considerations yield the expression for the combination of x' and y' components of the photocurrent which follows from Eqs. (4) for $E_z = 0$

$$j_{x'} + \mathrm{i}j_{y'} = \mathrm{i}\chi'(E_{x'} - \mathrm{i}E_{y'})(E_{x'}^* - \mathrm{i}E_{y'}^*)\exp(3\mathrm{i}\Phi)$$

or, equivalently,

$$j_{x'} = \chi'(t_0 E_0)^2 \sin(2\alpha - 3\Phi), \qquad \text{(A1)}$$
$$j_{y'} = \chi'(t_0 E_0)^2 \cos(2\alpha - 3\Phi),$$

where α is counted from y': $\boldsymbol{E}(\alpha = 0) \parallel y'$.

Equations (A1) demonstrate that the azimuth angular dependence for arbitrary orientation of contacts in respect to the crystallographic directions remains the same but differs by the phase shift 3Φ.

Finally we note that the photocurrent determined by the constant χ in Eqs. (4) is independent of the angle Φ because it is totally defined by position of the incidence plane and polarization of light. Therefore Eqs. (7) holds for any angle Φ.

APPENDIX B: DERIVATION OF INTERBAND MATRIX ELEMENTS

Equation (23) can be obtained from the two-band electron effective Hamiltonian

$$\mathcal{H}_{c\Gamma_1;v,\Gamma_{6x}}(\boldsymbol{k}) = \frac{\hbar}{m_0}(\mathrm{i}\mathcal{P}k_x + \mathcal{Q}k_x k_y), \qquad \text{(B1)}$$
$$\mathcal{H}_{c\Gamma_1;v,\Gamma_{6y}}(\boldsymbol{k}) = \frac{\hbar}{m_0}\left[\mathrm{i}\mathcal{P}k_y + \mathcal{Q}\frac{1}{2}(k_x^2 - k_y^2)\right],$$

by using the relation

$$\boldsymbol{e} \cdot \boldsymbol{p}_{c\Gamma_1;v,\Gamma_6}(\boldsymbol{k}) = \frac{m_0}{\hbar}(\boldsymbol{e} \cdot \nabla_{\boldsymbol{k}})\mathcal{H}_{c\Gamma_1;v,\Gamma_6}(\boldsymbol{k}).$$

We describe the symmetry reduction from C_{6v} to C_{3v} by introducing a δ-functional perturbation $\hat{V}'\delta(z - z_{\mathrm{if}})$, where z_{if} is the interface coordinate in the z axis and the operator $\hat{V}'$ transforms according to the representation B_1 of the group C_{6v} with the basic function $y^3 - 3x^2y$ (here as before we assume that one of the three mirror-reflection planes in the C_{3v} group contains the axes y, z and is perpendicular to x). The perturbation $\hat{V}'$ mixes the Bloch state Γ_6 with Γ_5 and the Bloch state Γ_3 with Γ_1.

In order to find the quadratic-in-$\boldsymbol{k}$ correction in Eq. (B1) we calculate the third-order correction to the Hamiltonian using the perturbation theory:[34]

$$\hat{\mathcal{H}}_{c;v}^{(3)} = \frac{1}{2} \sum_{ss'} \hat{\mathcal{H}}_{c;s} \hat{\mathcal{H}}_{s,s'} \hat{\mathcal{H}}_{s'v} \Phi(ss') \,,$$

$$\Phi(ss') = \left[\frac{1}{(E_c^0 - E_s^0)(E_c^0 - E_{s'}^0)} + \frac{1}{(E_v^0 - E_s^0)(E_v^0 - E_{s'}^0)} \right] \,.$$

Here the indices c, v mean, respectively, the lowest conduction and the highest valence bands of the symmetry Γ_1 and Γ_6; s, s' are other conduction or valence bands different from c and v (the electron spectrum throughout the Brillouin zone for bulk GaN can be found, e.g., in Refs. 35,36). $\hat{\mathcal{H}}_{n,n'}$ is the matrix of the first-order matrix elements of the $\boldsymbol{k}\cdot\boldsymbol{p}$ coupling or the interface mixing between the states in the bands n and n'; E_n^0 is the electron energy in the band n at the Γ point. The dimension of the matrix $\hat{\mathcal{H}}_{n,n'}$ is $N \times N'$ where N, N' are degeneracies of the bands n and n', respectively. Taking into account the bands $s\Gamma_6$ ($s \neq v$), $s'\Gamma_5$ and $s''\Gamma_3$ we can present the coefficient $\mathcal{Q}$ in Eq. (B1) for a structure with a single interface in the following form

$$\mathcal{Q} = \mathcal{V}\delta(z - z_{\text{if}}) \,, \tag{B2}$$

$$\mathcal{V} = \frac{\hbar}{m_0} \left[P'(R'V_2 - V_1 R)\, \Phi(ss') - V_3 P''R\, \Phi(s''s') \right] \,.$$

The set of matrix elements is defined as follows:

$$V_1 = \langle s, \Gamma_{6x} | \hat{V}' | s', \Gamma_{5x} \rangle \,, \quad V_2 = \langle v, \Gamma_{6x} | \hat{V}' | s', \Gamma_{5x} \rangle \,,$$

$$V_3 = \langle c, \Gamma_1 | \hat{V}' | s'', \Gamma_3 \rangle \,,$$

$$P' = -\mathrm{i}\langle c, \Gamma_1 | p_x | s, \Gamma_{6x} \rangle \,, \quad P'' = -\mathrm{i}\langle s'', \Gamma_3 | p_x | s', \Gamma_{5x} \rangle \,,$$

$$R = -\mathrm{i}\langle s', \Gamma_{5x} | p_x | v, \Gamma_{6x} \rangle \,, \quad R' = -\mathrm{i}\langle s', \Gamma_{5x} | p_x | s, \Gamma_{6x} \rangle \,.$$

For the band $s'\Gamma_5$ we choose the basis $|s, \Gamma_{5x}\rangle$, $|s, \Gamma_{5y}\rangle$ which transforms under operations of the C_{3v} group as the coordinates x and y, i.e., as functions $|s', \Gamma_{6x}\rangle$, $|s', \Gamma_{6y}\rangle$. While deriving Eq. (B2) we took into account the relation between matrix elements imposed by the symmetry, e.g., $\langle c, \Gamma_1 | p_y | s, \Gamma_{6y} \rangle = \langle c, \Gamma_1 | p_x | s, \Gamma_{6x} \rangle$, $\langle c, \Gamma_{5y} | p_x | s, \Gamma_{6x} \rangle = -\langle c, \Gamma_{5y} | p_y | s, \Gamma_{6y} \rangle = \langle c, \Gamma_{5x} | p_x | s, \Gamma_{6x} \rangle$ etc.

It follows then that, for a heterojunction, the interband optical matrix elements are indeed given by Eq. (23) where

$$\mathcal{P} = P \int f_e(z) f_h(z) dz \,, \quad \mathcal{Q} = \mathcal{V} f_e(z_{\text{if}}) f_h(z_{\text{if}}) \,, \tag{B3}$$

$P = -\mathrm{i}\langle c, \Gamma_1 | p_x | v, \Gamma_{6x} \rangle = -\mathrm{i}\langle c, \Gamma_1 | p_y | v, \Gamma_{6y} \rangle$, and $f_e(z)$, $f_h(z)$ are the electron and hole envelope functions.

[1] H. Linke (ed.), *Ratchets and Brownian Motors: Basic Experiments and Applications*, special issue Appl. Phys. A: Mater. Sci. Process. A **75**, 167 (2002).

[2] A. M. Glass, D. von der Linde, and T. J. Negran, Appl. Phys. Lett. **25**, 233 (1974).

[3] B. I. Sturman and V. M. Fridkin, *The Photovoltaic and Photorefractive Effects in Noncentrosymmetric Materials* (Gordon and Breach, Philadelphia, 1992).

[4] E. L. Ivchenko, *Optical Spectroscopy of Semiconductor Nanostructures* (Alpha Science International, Harrow, UK, 2005).

[5] V. I. Belinicher, E. L. Ivchenko, and B. I. Sturman, Zh. Eksp. Teor. Fiz. **83**, 649 (1982) [Sov. Phys. JETP **56**, 359 (1982)].

[6] N. A. Sinitsyn, J. Phys.: Condens. Matter **20**, 023201 (2008).

[7] W. Weber, S. D. Ganichev, Z. D. Kvon, V. V. Bel'kov, L. E. Golub, S. N. Danilov, D. Weiss, W. Prettl, H.-I. Cho, and J.-H. Lee, Appl. Phys. Lett. **87**, 262106 (2005).

[8] W. Weber, S. D. Ganichev, S. Seidl, V. V. Bel'kov, L. E. Golub, W. Prettl, Z. D. Kvon, Hyun-Ick Cho, and Jung-Hee Lee, AIP Conf. Proc. **893**, 1311 (2007).

[9] X. W. He, B. Shen, Y. Q. Tang, N. Tang, C. M. Yin, F. J. Xu, Z. J. Yang, G. Y. Zhang, Y. H. Chen, C. G. Tang, and Z. G. Wang, Appl. Phys. Lett. **91**, 071912 (2007).

[10] Y. Q. Tang, B. Shen, X. W. He, K. Han, N. Tang, W. H. Chen, Z. J. Yang, G. Y. Zhang, Y. H. Chen, C. G. Tang, Z. G. Wang, K. S. Cho, and Y. F. Chen, Appl. Phys. Lett. **91**, 071920 (2007).

[11] K. S. Cho, C.-T. Liang, Y. F. Chen, Y. Q. Tang, and B. Shen, Phys. Rev. B **75**, 085327 (2007).

[12] W. Weber, S. Seidl, V. V. Bel'kov, L. E. Golub, E. L. Ivchenko, W. Prettl, Z. D. Kvon, Hyun-Ick Cho, Jung-Hee Lee, and S. D. Ganichev, Solid State Comm. **145**, 56 (2008).

[13] S. Nakamura and G. Fasol, *The Blue Laser Diode. GaN Based Light Emitters and Lasers*, (Springer, Berlin, 1997).

[14] S. D. Ganichev and W. Prettl, *Intense Terahertz Excitation of Semiconductors* (Oxford University Press, Oxford, 2006).

[15] G. M. H. Knippels, X. Yan, A. M. MacLeod, W. A. Gillespie, M. Yasumoto, D. Oepts, and A. F. G. van der Meer, Phys. Rev. Lett. **83**, 1578 (1999).

[16] K. Seeger, *Semiconductor Physics* (Springer, Wien, 1997).

[17] N. V. Smith, Phys. Rev. B **64**, 155106 (2001).

[18] K. S. Cho, Tsai-Yu Huang, Hong-Syuan Wang, Ming-Gu Lin, Tse-Ming Chen, C.-T. Liang, Y. F. Chen, and Ikai Lo, Appl. Phys. Lett. **86**, 222102 (2005).

[19] N. Tang, B. Shen, M. J. Wang, K. Han, Z. J. Yang, K. Xu, G. Y. Zhang, T. Lin, B. Zhu, W. Z. Zhou, and J. H. Chu, Appl. Phys. Lett. **88**, 172112 (2006).

[20] N. Thillosen, Th. Schäpers, N. Kaluza, H. Hardtdegen, and V. A. Guzenko, Appl. Phys. Lett. **88**, 022111 (2006).

[21] S. Schmult, M. J. Manfra, A. Punnoose, A. M. Sergent, K. W. Baldwin, and R. J. Molnar, Phys. Rev. B **74**, 033302 (2006).

[22] R. Cingolani, A. Botchkarev, H. Tang, H. Morkoc, G. Traetta, G. Coli, M. Lomascolo, A. Di Carlo, F. Della Sala, and P. Lugli, Phys. Rev. B **61**, 2711 (2000).

[23] V. I. Litvinov, Phys. Rev. B **68**, 155314 (2003).

[24] M. Born and E. Wolf, *Principles of Optics* (Pergamon Press, Oxford, 1970).

[25] L. I. Magarill and M. V. Entin, Fiz. Tverd. Tela **31**, 37 (1989) [Sov. Phys. Solid State **31**, 1299 (1989)].

[26] E. L. Ivchenko and G. E. Pikus, *Superlattices and Other Heterostructures. Symmetry and Optical Phenomena*, Springer Series in Solid State Sciences, Vol. 110 (Springer-Verlag, Heidelberg, 1995, 2nd ed. 1997).

[27] N. A. Sinitsyn, Q. Niu, and A. H. MacDonald, Phys. Rev. B **73**, 075318 (2006).

[28] S. A. Tarasenko, Pis'ma v ZhETF **85**, 216 (2007) [JETP Letters **85**, 182 (2007)].

[29] S. A. Tarasenko, Phys. Rev. B **73**, 115317 (2006).

[30] E. V. Beregulin, S. D. Ganichev, K. Yu. Glukh, Yu. B. Lyanda-Geller, and I. D. Yaroshetskii, Fiz. Tverd. Tela **30**, 730 (1988) [Sov. Phys. Solid State **30**, 418 (1988)].

[31] U. Rössler and J. Kainz, Solid State Commun. **121**, 313 (2002).

[32] L. E. Golub and E. L. Ivchenko, Phys. Rev. B **69**, 115333 (2004).

[33] E. V. Beregulin, S. D. Ganichev, K. Yu. Gloukh, Yu. B. Lyanda-Geller, and I. D. Yaroshetskii, Fiz. Tverd. Tela **31**, 115 (1989) [Sov. Phys. Solid State **31**, 63 (1989)].

[34] G. L. Bir and G. E. Pikus, *Symmetry and Strain-Induced Effects in Semiconductors* (Wiley, New York, 1974).

[35] Zhongqin Yang and Zhizhong Xu, Phys. Rev. B **54**, 17577 (1996).

[36] R. Beresford, J. Appl. Phys. **95**, 6216 (2004).